Sweat Resistant Silk Fibroin-based Double Network Hydrogel Adhesives

Jilei Wang[1,7], Nan Zhang[2,7], Yurong Tan[1], Fanfan Fu[1], Gengxin Liu[3], Yin Fang[4],

Xin-xing Zhang[5], Minsu Liu[6], Yuan Cheng[6,7]*, Jing Yu[1]*

1. School of Materials Science and Engineering, Nanyang Technological University, 639798, Singapore.
2. School of Chemistry and Chemical Engineering, Xi'an University of Science and Technology, 710054, Xi'an, P. R. China.
3. State Key Laboratory for Modification of Chemical Fibers and Polymer Materials, Center for Advanced Low-dimension Materials, College of Material Science and Engineering, Donghua University, Shanghai 201620, China.
4. School of Chemical and Biomedical Engineering, Nanyang Technological University, 637459, Singapore
5. School of Physics, Dalian University of Technology, Dalian 116024, P. R. China.
6. Monash Suzhou Research Institute, Monash University, Suzhou Industrial Park, Suzhou 215000, PR China
7. Department of Materials Science and Engineering, Monash University, VIC 3800, Australia.
8. These authors contribute equally.

* Corresponding authors.
Email address: Y. C. (yuan.cheng@monash.edu), J. Y. (yujing@ntu.edu.sg).

Abstract

The adhesion between flexible epidermal sensors and human skin is essential for maintaining the stable functionality of the sensors. However, it is still challenging for epidermal electronic devices to achieve durable adhesion to the surface of the skin, especially under sweaty or humid conditions. Here, we report a silk fibroin - polyacrylamide (SF-PAAm) double network (DN) hydrogel adhesive with excellent biocompatibility, strong and durable adhesion on wet surfaces, and tunable adhesive properties. The hydrophilic PAAm network greatly improves the water retention capability of the DN hydrogel and reduces the β-sheet crystalline content of the SF, leading to excellent adhesive properties of the hydrogel across a wide range of humidity. The SF-PAAm DN hydrogel adhesive can be readily integrated with different epidermal sensor arrays and performs very well in real-time on-body sweat sensing. The SF-PAAm DN hydrogels have great potential for various epidermal healthcare sensors as well as medical adhesives for other medical applications.

Key words: silk fibroin, adhesive, double network hydrogel, sweat resistant, hydrogen bonds

INTRODUCTION

Personalized healthcare monitoring becomes increasingly important nowadays due to the global aging population and more prevalent chronic diseases,[1-3] which poses a heavy burden on our healthcare system. Epidermal wearable devices represent a portable, non-intrusive and continuous method for providing reliable personalized health monitoring.[4-6] To obtain accurate human biophysical and biochemical information through the skin surface, the adhesion between the skin surface and the devices is critical. However, it is still challenging for epidermal electronic devices to achieve durable adhesion to the rough, soft, and textured surface of the skin.[7-10] This challenge is further amplified in hot and humid environments and/or during exercise, in which the sweat and movement of the human body may cause adhesive failure (detachment) of many artificial pressure-sensitive's adhesives.[11-13] Developing moisture-resistant pressure-sensitive adhesives is therefore critical for the flexible epidermal electronic sensors for personalized healthcare.

It is critical to achieving a suitable range of adhesion between the adhesives (e.g. medical tape and plastic bandages) and the surface of the skin. Weak adhesion can lead to the failure of the adhesives while too strong adhesion can lead to uncomfortable feelings such as sharp pain during the removal of the devices. To date, mussel-inspired and plant-inspired hydrogel adhesives based on nucleobases, zwitterionic polymers, and other synthetic materials have been developed.[14-20] Ideal adhesives should provide performance including tough hydrogel adhesion and non-destructive separation properties in multiple processes, or even on a wet surface.[21] However, there are currently few reports on functional hydrogel adhesives that obtain strong adhesion on wet tissue surfaces.[22]

Biocompatibility is another important consideration for developing skin adhesives for epidermal flexible electronics.[23] Contact anaphylaxis is the most common symptoms caused by current commercialized medical adhesives containing synthetic polymers.[24] Silk fibroin (SF) protein, with excellent biocompatibility and biodegradability, has been widely employed as protein-based substrates, dielectrics of transistors, and water-soluble sacrificial layers.[25-29] Recently, calcium-modified SF was used as an adhesive for epidermal electronics.[30-31] However, natural SF suffers from poor gel quality and efficiency.[32] More importantly, the structure of pristine SF hydrogels heavily depends on the water content of the hydrogel due to its high crystalline β-sheet contents, which render unstable mechanical properties of the hydrogel. Such drawbacks significantly limit the application of SF as an adhesive in various

medical applications.[33] The -$CONH_2$ group in Polyacrylamide (PAAm) has been reported that it can be hydrolyzed into COO^-, which will extend the polymer chain and absorb large amount of water.[34] PAAm are bioinert, biocompatible, and hydrophilic, making them useful as a complementary material to SF proteins.

Herein, we report a SF - polyacrylamide (SF-PAAm) double network (DN) hydrogel adhesives. The SF-PAAm hydrogel shows excellent adhesive properties, including strong and tunable adhesion on skin surfaces, good performance in a wide range of humidity, and excellent biocompatibility. The fabricated SF-PAAm double network hydrogel adhesives can be readily integrated with different sensor arrays coupling with signal collection and transmission circuit components, performed well in real-time on-body sweat sensing. This work provides a great adhesive candidate for various epidemic sensor and device applications, as well for the people with sensitive skins and athletes.

RESULTS AND DISCUSSION

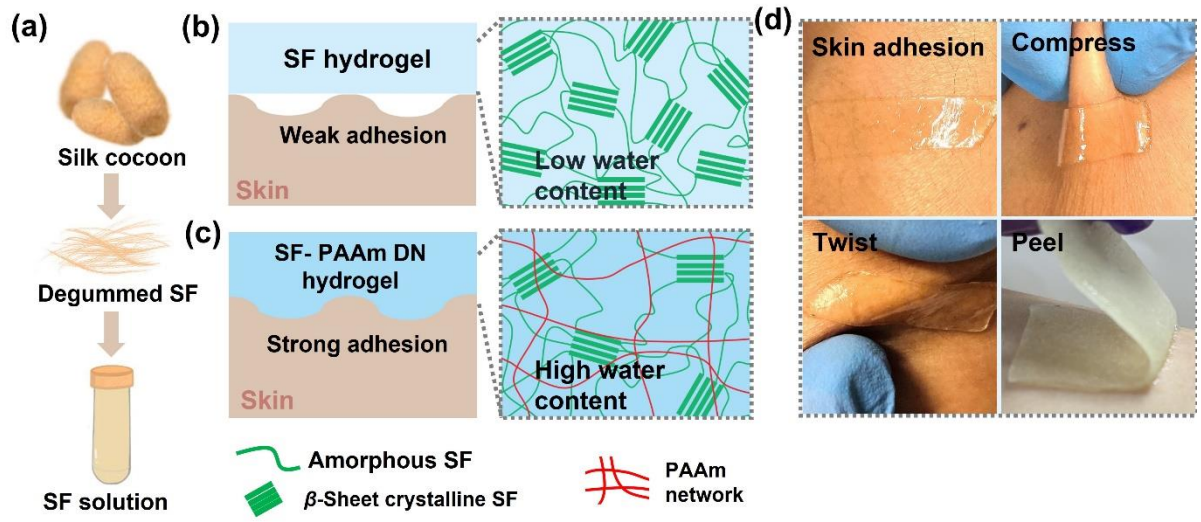

Figure 1. SF-PAAm hydrogel adhesives. (a) Preparation of SF solution. (b) Pristine SF hydrogel show poor adhesion on the skin surface under dry conditions, gaps exist at the interface due to low conformability. (c) SF-PAAm DN hydrogel can effectively maintain high water content and achieve strong and intimate adhesion on the skin surface. (d) Pictures of the SF-PAAm hydrogel on human skin surface under compression, twisting, and peeling motion.

We developed an SF-PAAm DN hydrogel with excellent water retention ability and strong adhesion on the skin surface. Pristine SF hydrogels with high water content possess good adhesive properties, but their inherent crystalline structure, poor water retention ability, and innately non-adhesiveness after drying can easily cause detachment of the SF hydrogel,

which greatly hamper their applications (Fig 1a, b). The introduced hydrophilic PAAm network greatly improves the water retention capability of the DN hydrogel and also reduces the β-sheet crystalline content of the silk fibroin (Fig. 1c), leading to low modulus and high conformability, and thus resulting in strong adhesion to the human skin. The SF-PAAm DN hydrogel can strongly adhere to the human skin surface and with stand various motion of the skin surface including compression and twisting (Fig. 1d).

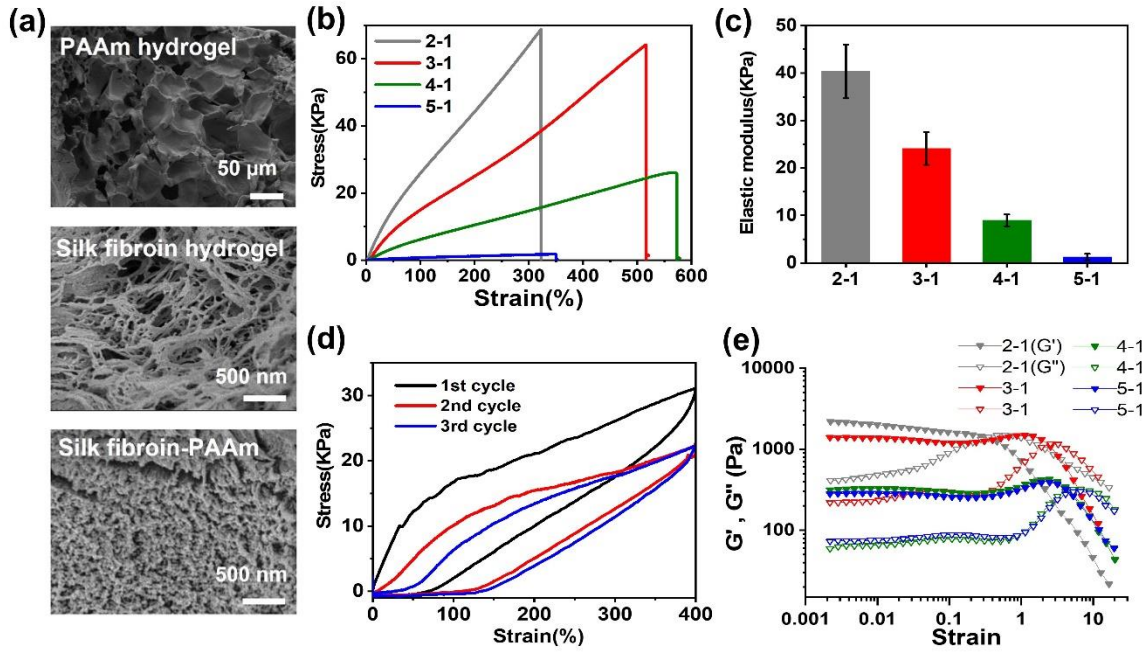

Figure 2. Properties of the SF-PAAm hydrogels. (a) Characteristic size scale and SEM images of pristine PAAm, SF and SF-PAAm hydrogels. (b) Stress-strain curves and (c) elastic moduli of SF-PAAm DN hydrogels with different SF/PAAm ratios. (d) The stress-strain curve of three continuous loading/unloading cycles of a SF-PAAm (4-1) DN hydrogel. (e) The storage and loss moduli of SF-PAAm DN hydrogels with different SF/PAAm radios as a function of shear strain.

Mechanical properties of the SF-PAAm adhesive hydrogels.

The SF-PAAm DN hydrogels possess excellent and tunable mechanical properties. SEM images on the cross-sectional morphology of pristine PAAm, pristine SF and SF-PAAm DN hydrogels after freeze-drying demonstrates that pristine PAAm and SF hydrogels exhibit porous and fibered structures, respectively. The characteristic size of the pristine PAAm network is on the order of ~ 30μm and the diameter of the SF fibre is on the order of ~ 100 nm. The hybrid assembly of PAAm and SF results in an interpenetrating DN hydrogel with high porosity (Fig. 2a). The maximum tensile strain of the SF-PAAm hydrogel before failure in a tensile stress-strain test increases from 320% to 580% increase of the SF/PAAm ratio from 2:1

to 4:1 (Fig.2b). However, upon increasing the SF/PAAm ratio increases to 5:1, the maximum strain decreases to 350%. Both the fracture stress and elastic modulus of the SF-PAAm hydrogel decrease with the increase of the SF content due to the relatively poor mechanical properties of the SF hydrogel network (Fig.2c). Continuous loading/unloading cycles tests of the stress-strain show the developed hydrogel having an obvious hysteresis phenomenon that's the typical characteristic of the double network structure of hydrogel (Fig.2d). Residual strain due to the viscoelasticity/viscoplasticity of the SF-PAAm hydrogel is also observed during the loading and unloading test with large stretch strain. The effect of the residual strain on the adhesion properties can be ignored since only 30% strength is required in practical applications.[35-37] The viscoelasticity/viscoplasticity of the SF-PAAm hydrogel is likely owing to the rupture and reforming of the hydrogen bonds in the crystalline domains of the silk fibroin. However, the hydrogel can recover part of the residual strain with sufficient time due to viscoelasticity (Fig. S1).

The dynamic mechanical properties of SF-PAAm DN hydrogel with different SF/PAAm ratios were evaluated as a function of angular frequency by rheological experiments. It is evident that for all compositions, their storage modulus G' were largely higher loss modulus G'', which indicates in the whole frequency range of linear viscoelastic region, the elastic behavior of these samples dominates over the viscous behavior for all the SF-PAAm hydrogels (Fig. S2). Both G' and G'' decrease as the SF content increases in the SF-PAAm gel. That is because the gel strength is mainly ascribed to strong chemical network formed by PAAm, while the SF only forms a relatively weak physical network. Similar trends were also observed when measuring G' and G'' as a function of strain (Fig. 2e). However, the maximum failure strain of the SF-PAAm gel increases as a function of the SF content.

Adhesive properties of the SF-PAAm hydrogel

We systematically characterized the adhesive properties of the SF-PAAm hydrogel adhesives. 180^{o} peeling forces of the hydrogel adhesives on a natural rubber substrate with different SF/PAAm weight ratios from 2:1 to 5:1 was measured by a tensile tester with a peeling speed of 5 mm/min and a relative humidity of 60% (Fig.3a, 3b). The adhesion of the DN hydrogel decreases while the mechanical property of the hydrogel increases with increasing the content of the covalently crosslinked PAAm. The adhesion is proportional to the content of the SF. High content of SF leads to large number of hydrogen bonds and thus high adhesion strength. Therefore, increasing the content of the PAAm in the hydrogel, namely decreasing

the content of SF will decrease the adhesion strength. To maintain a balance between the mechanical and adhesive properties of the SF-PAAm hydrogel, we fixed the SF/PAAm weight ratio at 4:1 and denoted as SF-PAAm hydrogel in the rest of the work.

SF is a classic biocompatible and eco-friendly material that has been widely explored in various biomedical applications. However, the inherent high crystallinity and poor water retention properties result in high modulus and low water content of pristine SF hydrogels, which hamper their applications. Pristine SF hydrogel needs to be kept at high relatively high humidities (>60%) in order to show strong adhesion, and samples kept at low humidities cannot adhere to a natural rubber surface. Contrarily, after 24 hours, the SF-PAAm hydrogel retains around 80% of the initial water content even at low (32%) humidity (Fig. S3), demonstrating the good water retention ability of our SF-PAAm hydrogel. In comparison, the SF-PAAm hydrogel possesses high adhesive force on rubber surface (~40-80 N/m) after storing 24 h at a wide range of relative humidity (32-98%) (Fig.3c). At 60% RH, the SF-PAAm hydrogel shows strong adhesion to different types of substrates, including PET, natural rubber, glass, SiO_2 and gold (Fig.3d).

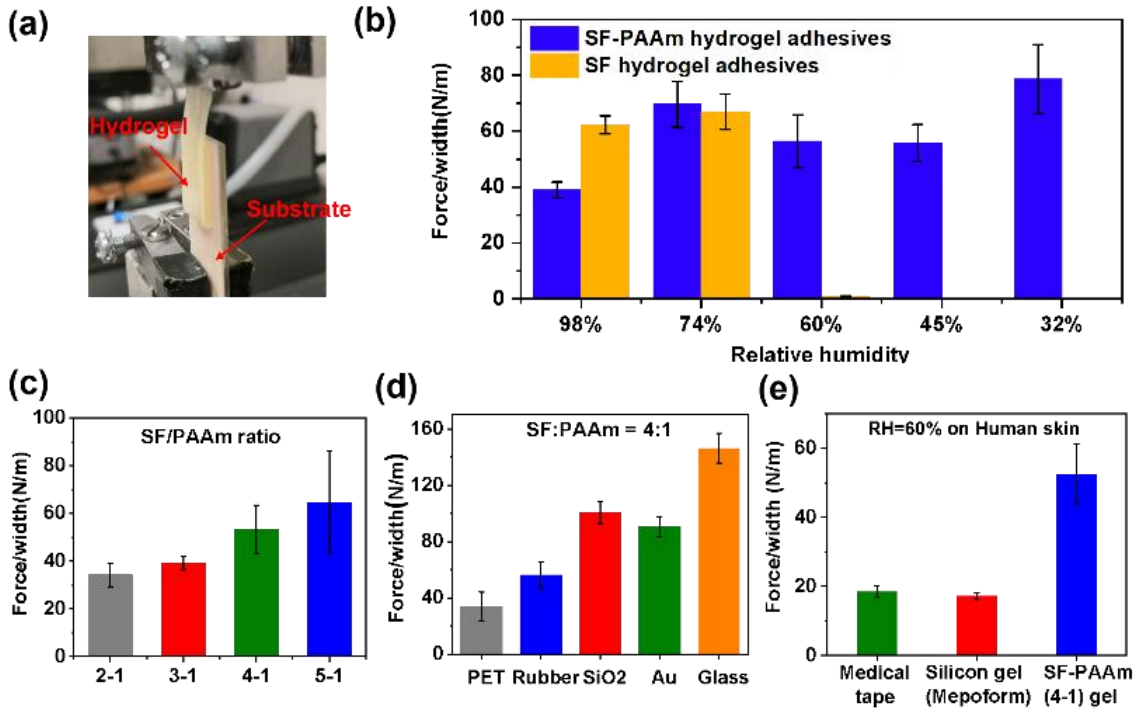

Figure 2. Adhesion of the SF-PAAm DN hydrogel. **(a)** Photograph of 180° peeling force measurement by a tensile tester. **(b)** 180° peeling adhesion forces of the pristine SF hydrogel and SF-PAAm DN hydrogel adhesives under different relative humidities. 180° peeling adhesion forces of the SF-PAAm DN hydrogel adhesives of **(c)** different SF/PAAm ratios and **(d)** substrates with SF-PAAm (4-1). **(e)** A comparison of the 180° peeling forces of commercial

medical tape, Silicone gel (Mepoform), and the SF-PAAm DN hydrogel (4-1) on human skin at a relative humidity of 60%. Three hydrogel samples were tested for all the peeling tests, and average values were reported with standard deviation.

The highest adhesion force of 146.3 N/m was measured on glass substrate due to the large amount of hydrogen bond formed by the SF protein and the glass surface, and the lowest adhesion force (34.0 N/m) measured on PET substrate. Compared with the commercial silicone gel (Mepoform) (~16.0 N/m) and medical tape (~18.0 N/m), the developed SF-PAAm hydrogel shows an average peeling force of 52.0 N/m on human skin (60%RH), which fully meets requirements of the majority of medical applications without causing injuries during peeling (Fig. 3e). The hydrogel adhesives patch can be completely peeled off from the skin without leaving any residue (Fig. S4). Such strong adhesive properties of the SF-PAAm hydrogel make it a great candidate as the adhesive for various applications requiring skin adhesives.

To exam the biocompatibility of the SF-PAAm hydrogel, we performed hematoxylin and eosin (H&E) stainings on pure SF hydrogel and SF-PAAm hydrogel. The prepared hydrogel samples were subcutaneous implanted in rats for 2 weeks. After being treated two weeks, pure SF hydrogel and SF-PAAm hydrogel groups showed similar degrees of inflammatory infiltration and fibroblast migration and proliferation, with rarely granulocytes, lymphocytes, and phagocytes infiltrated (Fig. S5), which indicates that the SF-PAAm hydrogel has very good biocompatibility similar to pristine silk hydrogel.

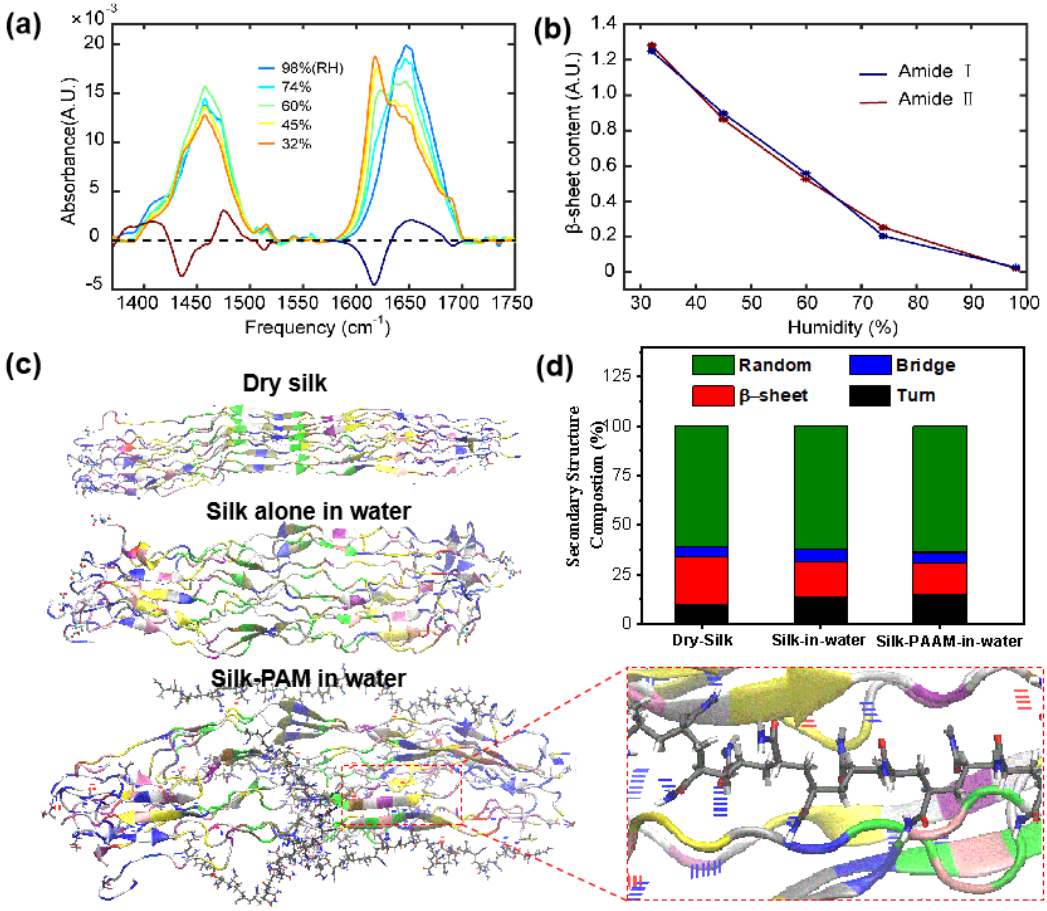

Figure 4. (a) ATR-FTIR spectra of the SF-PEGDA DN hydrogel with 4:1 SF/PEGDA weight ratio and the corresponding spectral components obtained using singular value decomposition (SVD) analysis. (b) The associated SVD amplitude components color-coded to the spectral one in (a). (c) Representative snapshots of MD simulations on dry SF protein, SF protein in water and SF -PAAm in water after equilibrium; The enlarged figure shows the hydrogen bonds between the SF and PAAm. (d) Contents of different secondary structures of dry SF protein, SF protein in water and SF -PAAm in water given by the MD simulation. Green, blue, red, and black represent the four types of secondary structures of random coil, isolated bridge, β-sheet and β-turn, respectively.

Conformational changes of SF protein

Attenuated total reflection-Fourier transform infrared (ATR-FTIR) spectroscopy was used to investigate the conformational changes of SF protein in the SF-PAAm double network hydrogel. Pure PAAm exhibits strong absorption centered at 1650 cm^{-1} assigned to the carbonyl stretch, which overlaps with the amide I region of SF (Fig. S6). For investigating the structural variation of the SF protein in the double network hydrogel, PEGDA was used instead of PAAm to avoid signal contamination. Fig.4a illustrates the ATR-FTIR spectra of the SF-PEGDA DN hydrogel with 4:1 SF/PEGDA weight ratio, showing the characteristic amide I and amide II

band of SF in the range of 1600-1700 and 1400-1500 cm^{-1}, respectively.[38] By increasing the relative humidity from 32 to 98%, the absorption peaks at 1617 and 1690 cm^{-1} disappear. The humidity-dependent global structural changes are then characterized by singular value decomposition (SVD). The obtained spectral component informs us the unfolding of β-sheet with increased humidity, with the intensity loss of the $\nu_{\perp}$ (1617 and 1490 cm^{-1}) and ν_{p} (1690 and 1435 cm^{-1}) vibrations of β-sheet. The signal increase at 1475 and 1653 cm^{-1} indicates the induced formation of α-helical structure with rising humidity. The associated amplitude components of both amide I and II region in Fig.4b, reveal a sharp conformational transition of SF in the humidity range from 32% to 74%, which is mainly due to the loss of β-sheet structures.

Influence of PAAm on structural change of silk protein

We performed all-atom molecular dynamic (MD) simulations to further understand the molecular interactions between PAAm polymer and SF, which were critical to the water retention and adhesive properties of the SF-PAAm hydrogel adhesives (Fig. 4c). The initial structure of selected SF contains rich *β*-sheet and random coils structures. To confirm the interaction mechanism between PAAm polymer and silk, we carried out three MD models of dry SF in vacuum, SF alone in water and SF-PAAm in water, respectively. The five PAAm polymer chains were randomly distributed around silk protein, and the number of repeating units of each PAAm polymer chain was 20. As shown in Fig. 4d, the β-sheet structure content was 24.18 ± 0.13% for a SF in vacuum. After the introduction of PAAm polymer, the average *β*-sheet structure content of silk protein decreased to 15.63 ± 0.10 %. The average content of random coil structure did not change significantly for the three systems (Dry SF: 61.06 ± 0.21%; SF-in-water: 62.22 ± 0.06%; SF-PAAm-in-Water: 63.73 ± 0.10%). In a word, the presence of water and PAAm polymer reduced the content of *β*-sheet structure, which is consistent with the results of the IR spectroscopy study.

Moreover, the stability of the protein secondary structure also depends on the hydrogen bonding interactions between the peptide chains in the silk protein. Therefore, to further elucidate the influence of water and PAAm on intra-molecular and inter-molecular hydrogen bonding status of silk, we showed the evolution of average number of hydrogen bonds (N_Hbond) with simulation time (Fig. S7), and also calculated the average N_Hbond of protein-water, intra-protein and protein-PAAM in a different system (Fig. S8). It can be found from Fig. S7 that the N_Hbond of SF protein was 260.80 ± 6.89 in the presence of water solvent,

and the N_Hbond of SF protein was 269.20 ± 8.42 in the presence of both water solvent and PAAm. Compared with dry SF protein (N_Hond): 342.00 ± 7.41), the loss rate of hydrogen bonding is 23.74% (Silk-in-water) and 21.28% (Silk-PAAm-in-Water). Besides, as shown in Fig. S8, the N_Hbond of silk and PAAM was 68.20 ± 6.50, which indicated that there was hydrogen bonding formed between PAAM and silk. Thus, both water solvents and PAAm can cause dissociation of the hydrogen bonds of silk protein.

Together, ATR-FRIR and MD simulation results reveal the critical role of the second PAAm network on the structure and functionality of the SF-PAAm DN hydrogel. The inherent high crystallinity and poor water retention properties of pristine SF result in high modulus low adhesion at a low humidity environment. Introducing a PAAm network can reduce the β-sheet crystalline content of the SF via disturbing the intra-molecular hydrogen bonding network of the protein, and thus improve the water retention capability of the fibroin protein. This leads to excellent adhesive properties of the SF-PAAm DN hydrogel across a wide range of humidity on different substrates, including human skin.

SF-PAAm DN hydrogel adhesive for sweat sensing

Due to the good biocompatibility and strong on-skin adhesion, the SF-PAAm DN hydrogel can serve as the adhesive for many applications that requires skin adhesives. To demonstrate such capability, we used the SF-PAAm DN hydrogel as the adhesive layer for an epidermal sweat sensor for on-body, real-time analysis on the concentrations of different ion species, including Na^+, K^+, Ca^{2+}, and pH of the sweat.

The integrated sweat sensor mainly includes four components from bottom to up, hydrogel adhesives layer, electrode/insulating layer, sensor layer and microchannel layer. Patterned microfluidic channels are designed for guiding the sweat passing through the electrochemical sensors. The integrated sensor is connected to an external circuit board working as a component for on-chip analysis of the sweat ion concentration, signal transduction, processing, and transmission using a blue tooth component, as shown in Fig. 5a, b. The highly integrated electrochemical sensor platform contains four functional sensors through decorating various ionophore-doped solvent polymeric membranes, allowing simultaneous detection of four health-related ions (Na^+, K^+, Ca^{2+} and pH) in human sweat.

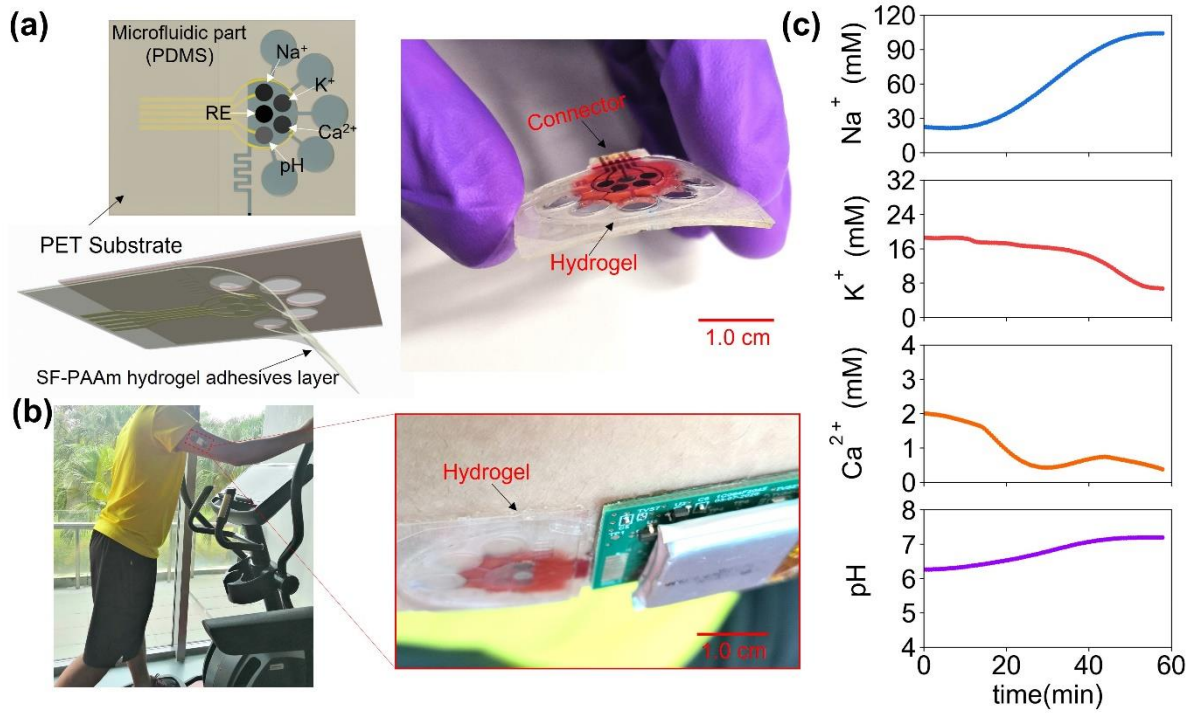

Figure 5. The SF-PAAm DN hydrogel adhesive is used as a sweat resistance adhesive for epidermal sweat sensors. (a) Schematic illustration of the various parts of a sweat sensor and corresponding photograph. The developed SF-PAAm DN hydrogel adhesive was used as the adhesive layer for the device. (b) Photograph of sweat sensor with the SF-PAAm DN hydrogel adhesives can adhere to the forearm of a person during excise for real-time, on-body sweat analysis. (c) The real-time sweat analysis results of the device adhered onto a subject's forearm during excise.

The SF-PAAm adhesive shows strong and durable adhesion on sweaty skin surfaces. During the running test, when the perspiration phenomenon was visually observed and the microchannel was filled with sweat solution (<15min), the stable data output could be realized. The on-body sweat analysis results of the device adhered onto a subject's forearm were shown in Fig. 5c. We measured the concentrations of Na^+, K^+ and Ca^{2+}ions, and the pH value of the sweat in real-time, which are important for monitoring the hydration state of the body. As a function of exercising time, Na^+ ion and pH value in the sweat gradually increased, while the concentrations of K^+ and Ca^{2+} slowly decreased during the exercise period. These monitored biological indicators all changed within normal physiological ranges, and the trends measured are consistent with the previous studies,[39-40] indicating that the developed SF-polymer hydrogel adhesives with high adhesion ability can be used for epidermal electronics applications with outstanding performance.

CONCLUSION

SF is a widely studied natural protein for various biomedical applications. However, due to the high crystalline β-sheet contents of pristine SF, the structure of SF hydrogels heavily depends on the water content of the hydrogel. The poor water retention ability of the SF hydrogel leads to unstable mechanical properties of the hydrogel, and limits the application of SF as adhesives in various applications. To overcome the inherent poor water retention ability of SF, we developed a SF-PAAm DN hydrogel strong water retention ability and tunable adhesive and mechanical properties. ATR-IR and MD simulation results show that the incorporation of the hydrophilic PAAm network can reduce the β-sheet crystalline content of the SF via disturbing the intra-molecular hydrogen bonding network of the protein, which greatly improve the water retention capability of the fibroin protein, resulting in strong and durable adhesion of the SF-PAAm hydrogel on various substrates across a wide range of humidity. With excellent biocompatibility, tunable mechanical properties, and strong adhesion on the human skin even under sweaty conditions, the SF-PAAm DN hydrogel can be used as medical adhesives for a variety of applications, including medical tapes and skin adhesives for flexible epidermal skin sensors for personalized healthcare.

MATERIALS AND METHODS

Materials

Raw bombyx mori silk fiber was purchased from Huzhou Yongrui Textile Co. Ltd. (Zhejiang Province, China). The monomer acrylamide (AAm), poly(ethylene glycol) diacrylateand (PEGDA) and the redox initiator ammonium persulfate (APS) were purchased from Aladdin company. Selectophore grade sodium ionophore X, valinomycin (potassium ionophore I), calcium ionophore II (ETH 129), 3,4-ethoxylenedioxythiophene (EDOT), poly(sodium 4-styrenesulfonate) (NaPSS), aniline, were purchased from Sigma-Aldrich. All other chemicals (analytical reagent grade) were commercially available and used without further purification. Ultrapure water (resistivity >18.0 MΩ.cm) was supplied by a Thermal-fisher water purification system and used for all experiments.

Characterization

^{1}H NMR spectra were recorded on a JEOL JNM-ECA 600 NMR spectrometer using DMSO-d_6 as the solvent and tetramethylsilane (TMS) as the internal standard. Attenuated Total

Reflection Flourier Transformed Infrared Spectroscopy (ATR-FTIR) measurements were performed using a Thermo-Nicolet 6700 FTIR spectrometer. Surface morphologies were characterized using a field-emission scanning electron microscope (SEM) from Zeiss corporation (Zeiss Merlin). The adhesion force and peeling forces tests were performed using a mechanical tester (C42, MTS Systems Corporation). Electrochemical measurements, CV and OCP measurements were carried out with a CHI760E workstation (CH Instruments Inc.).

Purification of SF

SF was purified as previously described.[41] First, to remove the sericin coating (degum), 10 g silk fiber was boiled in 0.02 M Na_2CO_3 distilled water solution for 1 h, and rinsed thoroughly with deionized water. Then, the degummed silk fiber was air-dried and dissolved in ethanol/water mixture solution (v/v, 4:5) with 5.0 M $CaCl_2$ at 60 ^oC for 2 h. The obtained solution was dialyzed against deionized water in a 3500 Da cutoff dialysis tube (VWR Scientific) for 3 days in an ice bath. The solution was centrifuged at 10000 rpm for 5 min to remove insoluble solids. SF was obtained by freeze-drying the supernatant and stored at 4°C when not in use.

Synthesis of SF-polymer DN hydrogel

The SF-polymer DN hydrogels were synthesized with the aid of high gel quality of PAAm and SF (Fig. S9). Firstly, 6.5 ml of a carefully degassed aqueous precursor solution (48.0 wt% SF, 12.0 wt% AM and 0.6 wt% APS) was mixed with 6 μL TEMED. Subsequently, the hydrogel precursor solution was poured into a reaction mold. Finally, the samples were put into an oven at 70 °C for 4 h to obtain the hydrogel adhesives. The obtained hydrogel was repeatedly immersed in high concentration of fresh SF aqueous solution for removing the residual monomer. Different weight ratios of SF-polymer adhesives can be easily regulated and the whole fabricate processes were similar to above mentioned. All hydrogels for mechanical characterizations had 2~3 mm thick, 10 mm wide, and height of 20 mm. After 4 hours, the 4:1 SF-PAAm hydrogel achieves an equilibrium swelling ratio of around 250% in DI water (Fig. S10).

Simulation Method

Structural optimization and parameterization of PAAm polymers

The geometric structure of PAAm polymer was constructed by GaussView 05 software.[42] First, Gaussian 16 program[43] was employed to preliminarily optimize the PAAm polymer

configuration and calculate the electrostatic potential by using the B3LYP/6-31G*(d) basis and the Hartree-Fork algorithm.[44-45] Secondly, to obtain the topology file of PAAm polymer, the Antechamber program in the Amber-Tools software package was used to fit the constrained electrostatic potential.[46-47] The generalized Amber force field (GAFF) to generate Amber structure and coordinate files. Finally, ACPYPE script in the Antechamber program was performed to convert the structural and topology files into Gromacs input file format, to prepare for the subsequent MD simulation.

Design and construction of PAAm-Silk system model

The complete sequence of heavy chain of SF protein contains 5000+ residues,[48] and its structure is not available in Protein Data Bank. In this study, we adopt the sequence of representative amorphous domain based on the SF sequence of the Linker 6 as published by Zhou et al: (GAGAGAGAGAGTGSSGFGPYVANGGYSGYEYAWSSESD FGTGS). The initial structure of silk consisted of 12 fully-extended chains aligned in an anti-parallel direction. The silk structure was pre-equilibrated in explicit water solvent. The pre-equilibrated silk protein contains rich β-sheet and random coils structures. To clarify the interaction mechanism between PAAM polymer and silk, we designed and built three scenarios: silk only in vacuum, silk alone in water solvent and PAAM-Silk in water solvent, respectively. In the PSV and PSW models, five PAAM polymer chains are randomly placed around the silk, which is consistent with PAAM-silk mass ratio adopted in experiments. In each simulation system, the initial coordinates of silk are located at the exact center of the simulation box filled with water, and the minimum cutoff distance of the solute from the simulation box is set to 1.2 nm. The dimensions of the simulation box are 8.72×7.77×17.10 nm^3, 6.41×7.43×17.45 nm^3, 17.96×17.96×17.96 nm^3, 6.41×7.43×17.45 nm^3, and the system contains 114494, 8258, 81707 atoms respectively. Each simulation system performs three repetitive calculations.

Molecular dynamics (MD) simulation method of PAAm-Silk interaction

In this study, GROMACS 5.1.2 [49] was used to perform molecular dynamics simulations on all PAAm-Silk systems, and the AMBER03 force field was used to parameterize silk.[50] Using the three-point solvent TIP3P water model,[51] each system uses 36 counterions (Na^+) to balance the system charges. Using V-rescale temperature controller, and the system temperature is set to 310K.[52] The Berendsen pressure coupling method [53] is used to describe the pressure, and the system pressure is set to 1 atm. The LINCS algorithm is used to limit the atomic bonds between PAAm polymer and silk.[54] The cutoff distance for non-bonding interactions is 1 nm. The

electrostatic interaction is processed by the particle grid Ewald method, and the cutoff distance is set to 1 nm.[55] The constructed systems are all studied using periodic boundary conditions. Before the dynamic simulation, the fastest descent algorithm is used to minimize the energy of the system. Secondly, through the NVT ensemble and NPT ensemble, the whole system is a pre-balanced simulation. After the temperature and pressure of the system are balanced, set the time step of the finished product simulation to 0.002 ps and the simulation time to 200 ns.

Rheological experiment

Rheological characterization was performed on MARS60, HAAKE (Thermo-Scientific, Germany) using 20 mm parallel plates. Linear response region tests were performed from strain of 0.001 to 20 at 25℃ and angular frequency of 10 rad/s. Small amplitude oscillatory shear (SAOS) measurements at 25℃ were performed at under constant stress (< 20Pa) within the linear response region.

Adhesion force and peeling force test

The adhesive peeling forces tests were performed using a mechanical tester (C42, MTS Systems Corporation). The samples were pre-placed into a humidity chamber overnight with controlled humidity (98-32%) using saturated salt solution. The test environmental humidity was ~60%, measured by a commercial humidity meter HI 9565 (HANNA Instruments). In the 180^{o} peeling force measurement, the hydrogels adhered onto a rubber film, and were then kept in a chamber with controlled ~60% humidity overnight. During the test, one the end of the rubber film was fixed on one clamp, the one end of the hydrogel (its back side was fixed on a flexible PET film) was clipped onto another clamp fixed on the load cell. The 180^{o} peeling forces between the samples and different substrates were measured at a speed of 5 mm/min. The adhesion strength G is related to the peeling force F, peeling angle θ and width of the sample w, by $G = F/w(1-\cos\theta)$. In this article, F/w values are compared between different samples (same peeling angle $\theta = \pi$).

Biocompatibility test in vivo

The biocompatibility property of the hydrogel was further confirmed in vivo in a rat model. The SF-polymer DN hydrogels were implanted subcutaneously on the back of SD rat (Xuebang Tech., Beijing, China). The pure SF hydrogels (produced by a methacrylation process using glycidyl methacrylate) were treated as a positive control. In the days following the surgical operation, the animal activity and appearance of the wound were examined each day. The

surgical sites were harvested to examine infections and inflammatory reactions. All experiments were approved by the Beijing Medi Siwei Biotechnology Co., Ltd. (SYXK-2020-0050).

Device integration and electrochemical measurements

The integrated sweat sensor mainly includes four components from bottom to up, hydrogel adhesives layer, electrode/insulating layer, sensor layer and microchannel layer. As for the hydrogel adhesives layer, homogeneous hydrogel precursor first infiltrate into a single side thin cellulose membrane (another side was covered with PE for bonding with device substrate). After degassing and gelation in given mold, the generated hydrogel layer was peeled off and punched five 4 mm diameter holes for interconnection of the microchannel part. The details of the sensor fabrication and calibration can be found in the supporting information. To attach the integrated sweat sensor to human skin, a medical-grade silicone gel (Mepiform) adhesive was used. Bluetooth app was used to connect the sweat sensor to a smart phone, which can record and display the test results in real-time. All experiments were approved by the Ethics Committee of Nanyang Technological University (Institutional Review Board (IRB) Protocol: IRB-2017-08-035).

Experimental repeats and statistical analyses

In order to assure the experimental repeats, Triplicates of specimens were measured in all experiments, where the collected values were averaged. Meanwhile, standard deviation was reported as the error bar on the plots.

ASSOCIATED CONTENT

Supporting Information

The supporting information includes: specific details on device integration and electrochemical measurements; additional information on the rheological and adhesion properties of SF/PAAm hydrogels and results on their biocompatibility; ATR-FTIR spectra on the chemical conformation of the samples in D_2O; MD simulation results regarding the effect of PAAm on the secondary structures.

AUTHOR INFORMATION

Corresponding Authors

Yuan Cheng - *Monash Suzhou Research Institute, Monash University, Suzhou Industrial Park, Suzhou, 215000, PR China*; orcid.org/0000-0003-0061-3934;

E-mail: yuan.cheng@monash.edu

Jing Yu - *School of Materials Science and Engineering, Nanyang Technological University, 639798, Singapore*; orcid.org/0000-0002-4288-951X;

E-mail: yujing@ntu.edu.sg

Authors

Jilei Wang - *School of Materials Science and Engineering, Nanyang Technological University, 639798, Singapore*; orcid.org/0000-0002-0950-0971;

Nan Zhang - *School of Chemistry and Chemical Engineering, Xi'an University of Science and Technology, 710054, Xi'an, P. R. China*; orcid.org/0000-0002-5412-8398;

Yurong Tan - *School of Materials Science and Engineering, Nanyang Technological University, 639798, Singapore*; orcid.org/0000-0002-1633-633X;

Fanfan Fu - *School of Materials Science and Engineering, Nanyang Technological University 639798, Singapore*; orcid.org/0000-0002-4443-9846;

Gengxin Liu - *State Key Laboratory for Modification of Chemical Fibers and Polymer Materials, Center for Advanced Low-dimension Materials, College of Material Science and Engineering, Donghua University, Shanghai 201620, China*; orcid.org/ 0000-0002-2998-8572;

Yin Fang - *School of Chemical and Biomedical Engineering, Nanyang Technological University, 637459, Singapore*; orcid.org/0000-0002-3415-6076;

Xin-xing Zhang - *School of Physics, Dalian University of Technology, Dalian 116024, P. R. China*; orcid.org/0000-0001-6974-4727;

Minsu Liu - *Monash Suzhou Research Institute, Monash University, Suzhou Industrial Park, Suzhou 215000, PR China*; orcid.org/0000-0003-0787-1725;

Author Contributions

JW, YT, and FF performed the hydrogel synthesis, adhesion measurements, sweat sensor fabrication, test, and data analysis. JW and GL performed the rheology measurements and data analysis. JW, YF, and ZX performed FTIR measurements and data analysis. NZ, ML, and YC

performed the molecular dynamics simulations and data analysis. YC and JY designed and supervised the research. JW, NZ, YT, ZX, YC and JY wrote the manuscript.

Notes

The authors declare no competing financial interest.

ACKNOWLEDGMENTS

J. Wang, F. Fu, Y. Tan, and J. Yu acknowledge the AME programmatic funding scheme of Cyber Physiochemical Interfaces (CPI) project #A18A1b0045 and the Singapore National Research Foundation Fellowship (NRF-NRFF11-2019-0004). X. Z. thanks to the support from Fundamental Research Funds for the Central Universities (DUT21RC(3)030).

REFERENCES

[1] Ungvari, Z.; Adany, R. The Future of Healthy Aging: Translation of Geroscience Discoveries to Public Health Practice. *Eur. J. Public Health* **2021**, 31 (3), 455-456.
[2] Egger, G.; Dixon, J. Beyond Obesity and Lifestyle: A Review of 21st Century Chronic Disease Determinants. *Biomed. Res. Int.* **2014**, 2014, 731685.
[3] Henney, A. M. The Promise and Challenge of Personalized Medicine: Aging Populations, Complex Diseases, and Unmet Medical Need. *Croat. Med. J.* **2012**, 53 (3), 207.
[4] Heikenfeld, J.; Jajack, A.; Rogers, J.; Gutruf, P.; Tian, L.; Pan, T.; Li, R.; Khine, M.; Kim, J.; Wang, J.; Kim, J. Wearable Sensors: Modalities, Challenges, and Prospects**.** *Lab on a Chip* **2018**, 18 (2), 217-248.
[5] Kim, J.; Campbell, A. S.; de Ávila, B. E.-F.; Wang, J. Wearable Biosensors for Healthcare Monitoring. *Nat. Biotechnol.* **2019**, 37 (4), 389-406.
[6] Chen, Y.; Zhang, Y.; Liang, Z.; Cao, Y.; Han, Z.; Feng, X. Flexible inorganic bioelectronics. *npj Flexible Electronics* **2020,** 4 (1), 2.
[7] Duan, J.; Xie, W.; Yang, P.; Li, J.; Xue, G.; Chen, Q.; Yu, B.; Liu, R.; Zhou, J. Tough Hydrogel Diodes with Tunable Interfacial Adhesion for Safe and Durable Wearable Batteries. *Nano Energy* **2018**, 48, 569-574.
[8] Amjadi, M.; Kyung, K. U.; Park, I.; Sitti, M. Stretchable, Skin-Mountable, and Wearable Strain Sensors and Their Potential Applications: A Review. *Adv. Funct. Mater.* **2016**, 26 (11), 1678-1698.
[9] Liu, X.; Liu, J.; Wang, J.; Wang, T.; Jiang, Y.; Hu, J.; Liu, Z.; Chen, X.; Yu, J. Bioinspired, Microstructured Silk Fibroin Adhesives for Flexible Skin Sensors. *ACS Appl. Mater. Interfaces* **2020**, 12 (5), 5601-5609.
[10] Lim, D.; Baek, M.; Kim, H.; Baig, C.; Dong W. Carboxyethyl Acrylate Incorporated Optically Clear Adhesives with Outstanding Adhesion Strength and Immediate Strain Recoverability for Stretchable Electronics. Chem. Eng. J. **2022**, 437, 135390.
[11] Wolf, M. P.; Salieb-Beugelaar, G. B.; Hunziker, P. PDMS with Designer Functionalities—Properties, Modifications Strategies, and Applications. *Prog. Polym. Sci.* **2018**, 83, 97-314.

[12] Singla, S.; Amarpuri, G.; Dhopatkar, N.; Blackledge, T. A.; Dhinojwala, A. Hygroscopic Compounds in Spider Aggregate Glue Remove Interfacial Water to Maintain Adhesion in Humid Conditions. *Nat. Commun.* 2018, 9 (1), 1890.
[13] Li, Q.; Chen, G.; Cui, Y.; Ji, S.; Liu, Z.; Wan, C.; Liu, Y.; Lu, Y.; Wang, C.; Zhang, N.; Cheng, Y.; Zhang, K.-Q.; Chen, X., Highly Thermal-Wet Comfortable and Conformal Silk-Based Electrodes for On-Skin Sensors with Sweat Tolerance. *ACS Nano* **2021,** *15* (6), 9955-9966.
[14] Kim, B. J.; Oh, D. X.; Kim, S.; Seo, J. H.; Hwang, D. S.; Masic, A.; Han, D. K.; Cha, H. J. Mussel-Mimetic Protein-Based Adhesive Hydrogel. *Biomacromolecules* **2014**, 15 (5), 1579-1585.
[15] Liu, X.; Zhang, Q.; Gao, G. Bioinspired Adhesive Hydrogels Tackified by Nucleobases. *Adv. Funct. Mater.* **2017**, 27, 1703132.
[16] Bai, S.; Zhang, X.; Lv, X.; Zhang, M.; Huang, X.; Shi, Y.; Lu, C.; Song, J.; Yang, H. Bioinspired Mineral–Organic Bone Adhesives for Stable Fracture Fixation and Accelerated Bone Regeneration. *Adv. Funct. Mater.* **2020**, 30, 1908381.
[17] Gan, D.; Xing, W.; Jiang, L.; Fang, J.; Zhao, C.; Ren, F.; Fang, L.; Wang, K.; Lu, X. Plant-Inspired Adhesive And Tough Hydrogel Based On Ag-Lignin Nanoparticles-Triggered Dynamic Redox Catechol Chemistry. *Nat. Commun.* **2019**, 10 (1), 1487.
[18] Blacklow, S. O.; Li, J.; Freedman, B. R.; Zeidi, M.; Chen, C.; Mooney, D. J.; Bioinspired Mechanically Active Adhesive Dressings to Accelerate Wound Closure. *Sci. Adv.* **2019**, 5 (7), eaaw3963.
[19] Yang, B.; Yuan, W. Highly Stretchable, Adhesive, and Mechanical Zwitterionic Nanocomposite Hydrogel Biomimetic Skin. *ACS Appl. Mater. Interfaces* **2019**, 11 (43), 40620-28.
[20] Li, J.; Celiz, A. D.; Yang, J.; Yang, Q.; Wamala, I.; Whyte, W.; Seo, B. R.; Vasilyev, N.; Vlassak, J.; Suo, Z.; Mooney, D. J. Tough Adhesives for Diverse Wet Surfaces. *Science* **2017**, 357, 378-381.
[21] Kim, D.-H.; Lu, N.; Ma, R.; Kim, Y.-S.; Kim, R.-H.; Wang, S.; Wu, J.; Won, S. M.; Tao, H.; Islam, A.; Yu, K. J.; Kim, T.-i.; Chowdhury, R.; Ying, M.; Xu, L.; Li, M.; Chung, H.-J.; Keum, H.; McCormick, M.; Liu, P.; Zhang, Y.-W.; Omenetto, F. G.; Huang, Y.; Coleman, T.; Rogers, J. A. Epidermal Electronics. *Science* **2011**, 333 (6044), 838-843.
[22] Karami, P.; Wyss, C. S.; Khoushabi, A.; Schmocker, A.; Broome, M.; Moser, C.; Bourban, P.-E.; Pioletti, D. P. Composite Double-Network Hydrogels to Improve Adhesion on Biological Surfaces. *ACS Appl. Mater. Interfaces* **2018**, 10 (45), 38692-99.
[23] Chung, H. U.; Kim, B. H.; Lee, J. Y.; Lee, J.; Xie, Z.; Ibler, E. M.; Lee, K.; Banks, A.; Jeong, J. Y.; Kim, J.; Ogle, C.; Grande, D.; Yu, Y.; Jang, H.; Assem, P.; Ryu, D.; Kwak, J. W.; Namkoong, M.; Park, J. B.; Lee, Y.; Kim, D. H.; Ryu, A.; Jeong, J.; You, K.; Ji, B.; Liu, Z.; Huo, Q.; Feng, X.; Deng, Y.; Xu, Y.; Jang, K.-I.; Kim, J.; Zhang, Y.; Ghaffari, R.; Rand, C. M.; Schau, M.; Hamvas, A.; Weese-Mayer, D. E.; Huang, Y.; Lee, S. M.; Lee, C. H.; Shanbhag, N. R.; Paller, A. S.; Xu, S.; Rogers, J. A. Binodal, wireless epidermal electronic systems with in-sensor analytics for neonatal intensive care. *Science* **2019,** 363 (6430), eaau0780.
[24] Mestach, L.; Huygens, S.; Goossens, A.; Gilissen, L. Allergic Contact Dermatitis Caused by Acrylic-Based Medical Dressings and Adhesives. *Contact Derm.* **2018**, 79 (2), 81-84.
[25] Kim, D.-H.; Viventi, J.; Amsden, J. J.; Xiao, J.; Vigeland, L.; Kim, Y.-S.; Blanco, J. A.; Panilaitis, B.; Frechette, E. S.; Contreras, D.; Kaplan, D. L.; Omenetto, F. G.; Huang, Y.; Hwang, K.-C; Zakin, M. R.; Litt, B. Dissolvable Films of Silk Fibroin for Ultrathin Conformal Bio-Integrated Electronics. *Nat. Mater.* **2010**, 9 (6), 511-517.
[26] Koh, L.-D.; Cheng, Y.; Teng, C.-P.; Khin, Y.-W.; Loh, X.-J.; Tee, S.-Y.; Low, M.; Ye, E.; Yu, H.-D.; Zhang, Y.-W. Structures, Mechanical Properties and Applications of Silk

Fibroin Materials. *Prog. Polym. Sci.* **2015**, 46, 86-110.
[27] Maxwell, R.; Costache, M. C.; Giarrosso, A.; Bosques, C.; Amin, S.; Optimizing Interactions between Soluble Silk Fibroin and Capryl Glucoside for Design of a Natural and High-Performance Co-Surfactant System. *Int J Cosmet Sci.* **2021**, 43 (1), 68-77.
[28] Gholipourmalekabadi, M.; Sapru, S.; Samadikuchaksaraei, A.; Reis, R. L.; Kaplan, D. L.; Kundu, S. C. Silk Fibroin for Skin Injury Repair: Where Do Things Stand? *Adv. Drug Deliv. Rev.* **2020**, 153, 28-53.
[29] Tao, H.; Brenckle, M. A.; Yang, M.; Zhang, J.; Liu, M.; Siebert, S. M.; Averitt, R. D.; Mannoor, M. S.; McAlpine, M. C.; Rogers, J. A.; Kaplan, D. L.; Omenetto, F. G. Silk-Based Conformal, Adhesive, Edible Food Sensors. *Adv. Mater.* **2012**, 24 (8), 1067-1072.
[30] Seo, J.-W.; Kim, H.; Kim, K.; Choi, S. Q.; Lee, H. J. Calcium-Modified Silk as a Biocompatible and Strong Adhesive for Epidermal Electronics. *Adv. Funct. Mater.* **2018**, 28 (36), 1800802.
[31] Chen, G.; Matsuhisa, N.; Liu, Z.; Qi, D.; Cai, P.; Jiang, Y.; Wan, C.; Cui, Y.; Leow, W. R.; Liu, Z.; Gong, S.; Zhang, K.-Q.; Cheng, Y.; Chen, X. Plasticizing Silk Protein for On-Skin Stretchable Electrodes. *Adv. Mater.* **2018**, 30 (21), 1800129.
[32] Zheng, H.; Zuo, B. Functional Silk Fibroin Hydrogels: Preparation, Properties and Applications. *J. Mater. Chem. B* **2021**, 9 (5), 1238-1258.
[33] Shen, Y.; Levin, A.; Kamada, A.; Toprakcioglu, Z.; Rodriguez-Garcia, M.; Xu, Y.; Knowles, T. P. J. From Protein Building Blocks to Functional Materials. *ACS Nano* **2021**, 15 (4), 5819-5837.
[34] Kim, S.; Iyer, G.; Nadarajah, A.; Frantz, J. M.; Spongberg, A. L., Polyacrylamide Hydrogel Properties for Horticultural Applications. *Int. J. Polym. Anal. Charact.* **2010,** *15* (5), 307-318.
[35] Chen, H.; Zhu, F.; Jang, K.-I.; Feng, X.; Rogers, J. A.; Zhang, Y.; Huang, Y.; Ma, Y. The equivalent medium of cellular substrate under large stretching, with applications to stretchable electronics. *Journal of the Mechanics and Physics of Solids* **2018,** 120, 199-207.
[36] Zhang, Y.; Wang, S.; Li, X.; Fan, J. A.; Xu, S.; Song, Y. M.; Choi, K.-J.; Yeo, W.-H.; Lee, W.; Nazaar, S. N.; Lu, B.; Yin, L.; Hwang, K.-C.; Rogers, J. A.; Huang, Y. Experimental and Theoretical Studies of Serpentine Microstructures Bonded To Prestrained Elastomers for Stretchable Electronics. *Adv. Funct. Mater.* **2014,** 24 (14), 2028-2037.
[37] Ma, Y.; Zhang, Y.; Cai, S.; Han, Z.; Liu, X.; Wang, F.; Cao, Y.; Wang, Z.; Li, H.; Chen, Y.; Feng, X. Flexible Hybrid Electronics for Digital Healthcare. *Adv. Mater.* **2020,** 32 (15), 1902062.
[38] DeFlores, L.P.; Ganim, Z.; Ackley, S. F.; Chung, H. S.; Tokmakoff, A. The Anharmonic Vibrational Potential and Relaxation Pathways of the Amide I and II Modes of N-Methylacetamide. *J. Phys. Chem. B.* **2006**, 110 (38), 18973-80.
[39] Gao, W.; Emaminejad, S.; Nyein, H.; Challa, S.; Chen, K.; Peck, A.; Fahad, H. M.; Ota, H.; Shiraki, H.; Kiriya, D.; Lien, D. H.; Brooks, G. A.; Davis, R. W.; Javey, A. Fully Integrated Wearable Sensor Arrays for Multiplexed In Situ Perspiration Analysis. *Nat.* **2016**, 529 (7587), 509-514.
[40] Xu, G.; Cheng, C.; Liu, Z.; Yuan, W.; Wu, X.; Lu, Y.; Low, S. S.; Liu, J.; Zhu, L.; Ji, D.; Li, S.; Chen, Z.; Wang, L.; Yang, Q.; Cui, Z.; Liu, Q. Battery-Free and Wireless Epidermal Electrochemical System with All-Printed Stretchable Electrode Array for Multiplexed In Situ Sweat Analysis. *Adv. Mater. Technol.* **2019**, 4 (7), 1800658.
[41] Rockwood, D. N.; Preda, R. C.; Yücel, T.; Wang, X.; Lovett, M. L.; Kaplan, D. L. Materials Fabrication from Bombyx Mori Silk Fibroin. *Nat. Protoc.* **2011**, 6 (10), 1612-1631.

[42] Dennington, R.; Keith, T.; Millam, J. *GaussView Version* 5; Semichem Inc.: Shawnee Mission, **2009**.
[43] Frisch, M.; Trucks, G.; Schlegel, H.; Scuseria, G.; Robb, M.; Cheeseman, J.; Scalmani, G.; Barone, V.; Petersson, G. *Gaussian 16 Rev.*; Gaussian Inc.: Wallingford CT, **2016**.
[44] Foresman, J. B.; Frisch, A. E. *Exploring Chemistry with Electronic Structure Methods: A Guide to using*; Gaussian Inc., Gyan Books Pvt. Ltd, **1996**.
[45] Jensen, F. *Introduction to computational chemistry*; John Wiley & Sons, Inc., **2017**.
[46] Wang, J.; Cieplak, P.; Kollman, P. A. How Well Does a Restrained Electrostatic Potential (RESP) Model Perform in Calculating Conformational Energies of Organic and Biological Molecules? *J. Comput. Chem.* **2000**, 21 (12), 1049-1074.
[47] Du, J.; Qiu, M.; Guo, L.; Yao, X. Selective Inhibition of HDAC1 by Macrocyclic Polypeptide for the Treatment of Glioblastoma: A Binding Mechanistic Analysis Based on Molecular Dynamics. *J. Biomol. Struct. Dyn.* **2019**, 37, 1628-1640.
[48] Zhou, C. Z.; Confalonieri, F.; Jacquet, M.; Perasso, R.; Li, Z. G.; Janin, J. Silk Fibroin: Structural Implications of a Remarkable Amino Acid Sequence. *Proteins* **2001**, 44 (2), 119-122.
[49] Hess, B.; Kutzner, C.; Van Der Spoel, D.; Lindahl, E. GROMACS 4: Algorithms for Highly Efficient, Load-Balanced, and Scalable Molecular Simulation. *J. Chem. Theory Comput.* **2008**, 4 (3), 435-447.
[50] Duan, Y.; Wu, C.; Chowdhury, S.; Lee, M. C.; Xiong, G.; Zhang, W.; Yang, R.; Cieplak, P.; Luo, R.; Lee, T.; Caldwell, J.; Wang, J.; Kollman, P. A Point-Charge Force Field for Molecular Mechanics Simulations of Proteins Based on Condensed-Phase Quantum Mechanical Calculations. *J. Comput. Chem.* **2003**, 24 (16), 1999-2012.
[51] Price, D. J.; Brooks III, C. L. A Modified TIP3P Water Potential for Simulation with Ewald Summation. *J. Chem. Phys.* **2004**, 121 (20), 10096.
[52] Bussi, G.; Donadio, D.; Parrinello, M. Canonical Sampling through Velocity Rescaling. *J. Chem. Phys.* **2007**, 126 (1), 014101.
[53] Berendsen, H. J. C.; Postma, J. P. M.; van Gunsteren, W. F.; DiNola, A.; Haak, J. R. Molecular Dynamics with Coupling to an External Bath. *J. Chem. Phys.* **1984**, 81 (8), 3684-3690.
[54] Hess, B.; Bekker, H.; Berendsen, H. J.; Fraaije, J. G. E. M. LINCS: A Linear Constraint Solver for Molecular Simulations. *J. Comput. Chem.* **1997**, 18 (12), 1463-1472.
[55] Darden, T.; York, D.; Pedersen, L. Particle Mesh Ewald: An N · Log(N) Method for Ewald Sums in Large Systems. *J. Chem. Phys.* **1993**, 98 (12), 10089-92.

TOC

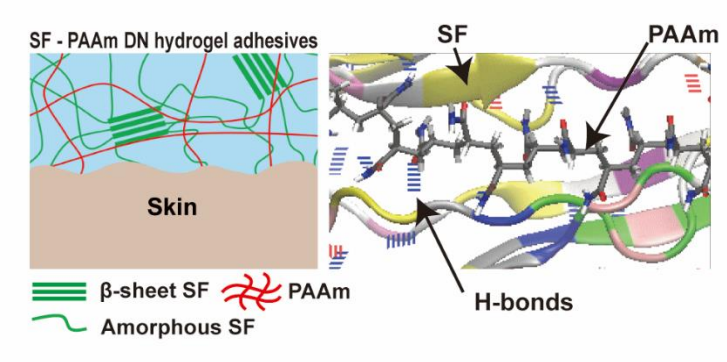
SF - PAAm DN hydrogel adhesives
Skin
β-sheet SF
PAAm
Amorphous SF
SF
PAAm
H-bonds